Miniaturized Pattern Formation in Elastic Films Cast on Sinusoidally Patterned Substrates

ARTICLE *in* LANGMUIR · SEPTEMBER 2014

Impact Factor: 4.46 · DOI: 10.1021/la502933c · Source: PubMed

2 AUTHORS:

Annepu Hemalatha

Indian Institute of Technology Delhi

4 PUBLICATIONS **10** CITATIONS

SEE PROFILE

Jayati Sarkar

Indian Institute of Technology Delhi

22 PUBLICATIONS **255** CITATIONS

SEE PROFILE

Langmuir

Article

pubs.acs.org/Langmuir

Miniaturized Pattern Formation in Elastic Films Cast on Sinusoidally Patterned Substrates

Hemalatha Annepu and Jayati Sarkar*

Chemical Engineering Department, Indian Institute of Technology Delhi, New Delhi 110 016, India

Supporting Information

ABSTRACT: The various morphologies that are formed when van der Waals forces or electric field is induced between film cast on a sinusoidal substrate and in contact proximity with a contactor or electrode are studied. Remarkably smaller length scales are achieved ($\lambda_c < 2.96h$) than those obtained with films cast on flat substrates. With van der Waals interactions, the patterns are uniformly formed throughout the film but are not regularly ordered. When electric field is used at critical voltage, more ordered, localized patterns are formed at the zones of large local interaction strengths. When these patterns are evolved by increasing the applied voltage, coexistence of all three phases—cavities, stripes, and columns—is observed throughout the film. The localized patterns that are initially formed vary with the voltage applied and strongly dictate the phases of evolution. A patterned substrate/patterned contactor assembly can be made to operate like its unpatterned counterpart by making the interaction strength same everywhere and yet yield uniform, regularly ordered, highly miniaturized patterns. Such patterns are very useful in various applications like microfluidics; they are formed with great ease and can be morphologically tuned by tuning the externally applied electric field.

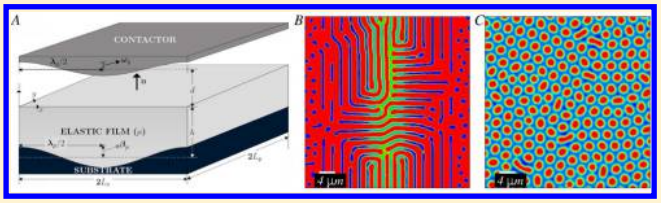

INTRODUCTION

Topographically patterned liquid and solid thin films exhibiting enhanced functional properties are important in numerous scientific applications like lab-on-chip devices for point-of-care clinical diagnosis,[1] stem cell scaffolds for tissue engineering,[2,3] functional coatings,[4] polymer membranes,[5] sensors,[6] thin film transistors,[7,8] solar batteries,[9] microfluidic mixers,[10] self-cleaning surfaces,[11,12] antireflective lens,[13] optical memory devices,[14] semiconductor microelectronics, and so forth,[15] and also serve as exemplary systems for understanding physical phenomena such as tunable adhesion, adhesion-debonding,[16−26] wetting−dewetting,[27−30] and so forth. Thin film patterning is achieved by mainly two different ways: top down approach and bottom up approach. The top down approach, consisting of various lithographic techniques such as electron beam lithography, dip-pen lithography, embossing lithography, and so forth, is expensive as well as inadequate in the patterning of soft elastic films.[31] The bottom up approach consists of self-assembly of molecules and self-organization techniques which aid in cost-effective bulk production of meso/nano structures[32] and thus are of greater interest for us to explore. Extensive literature exists in the area of morphological patterning of soft elastic surfaces in adhesive contact or in peeling configuration in close proximity with an external contactor where patterns formed are of length scales $3h$ or $4h$ depending on the contactor-film configuration and are independent of the nature of interactions present between the film and the contactor and the elastic modulus of the film.[16−35] In yet another work on hydrogel sandwiched between rigid plates, length scales $7h$ have been observed, and it is proposed that these large length scales can affect the fracture modes as well as the adhesive strength of the hydrogel.[36] There has been a lot of interest lately in forming miniaturized elastic film patterns of length scales less than $\sim 3h$ by various methods like elastic bilayers[37−41] and using topographically patterned substrates.[42−44] Recent works on using a patterned substrate have suggested that patterned substrates yield reduced length scale patterns due to the lateral variation in film thickness which results in lateral variation in elastic film stiffnesses.[43,44]

If the effects of van der Waals interactions are made negligible by increasing the air gap d between the film and the contactor and electric field is introduced instead, the strength of the destabilizing interactions varies laterally[23,30,45−55] because of the lateral variation in thicknesses during evolution of such films. Exposing the films cast on flat substrates to electric field instead of van der Waals interactions had proved to produce patterns which still scaled as $3h$ but were highly ordered compared to the labyrinthine patterns obtained from van der Waals interactions.[56] If there was an interplay between these two, that is, lateral variation of elastic stiffnesses (by using a patterned substrate) and lateral variation in interaction stiffness (by introducing electric field between substrate and contactor) it raises some interesting questions, would it result in further shrinking of length scales, will the patterns thus formed be uniformly distributed laterally or be concentrated at the zones of largest local interaction stiffnesses, and will the patterns still be well-ordered? First and foremost, we explore and address all

Received: July 27, 2014
Revised: September 17, 2014
Published: September 19, 2014

these possibilities in the present work with sinusoidally patterned substrates.

Patterned contactors have so far been used only as templates to form localized lateral patterns and never ensue reduction in pattern length scales.[21,57] This work takes a step forward in this direction by using a special sinusoidally patterned substrate/sinusoidally patterned contactor assembly to produce highly miniaturized patterns, with uniform lateral spread, for the first time. A two-dimensional (2D) nonlinear finite element analysis of elastic films cast on step and sinusoidally patterned substrates was performed earlier which provided valuable insights into understanding of length scales formed for adhesive films undergoing deformations due to van der Waals interactions.[44] It, however, does not prove to be useful in predicting the exact morphological phases in the three-dismensional (3D) space, more so for electric fields which now have a strong lateral variation in the interaction strength even before evolution. In the present work, we study, with the help of 3D nonlinear energy minimization simulations, the patterns formed on elastic films in contact proximity with an external contactor and under the influence of van der Waals interactions at critical gap distance as well as electrostatic interactions at different voltages for fixed gap distances.

MATHEMATICAL MODELING

Figure 1 shows the schematic of an initially stress-free, soft (shear modulus, μ < 1 MPa), thin (mean film thickness, h < 10 μm),

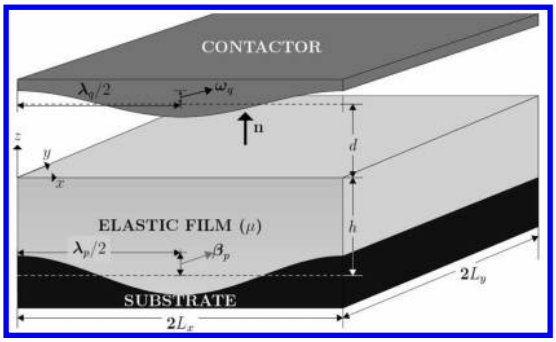

Figure 1. Three-dimensional schematic of a soft, incompressible elastomeric film rigidly bounded to a sinusoidally patterned substrate. The film is under the influence of a rigid sinusoidally patterned contactor situated at a gap distance d away from the stable flat surface of the elastic film. The mean thickness of the film is h, shear modulus μ, and lateral dimensions $2L_x$ and $2L_y$. The substrate pattern is defined by the amplitude β_p and wavelength λ_p, while the contactor pattern is defined by the amplitude ω_q and wavelength λ_q.

incompressible elastic film cast on a unidirectionally patterned sinusoidal substrate and under the influence of a rigid unidirectionally patterned sinusoidal contactor situated at a mean gap distance d away from the stable flat surface of the elastic film. The coordinate system used for the analysis is depicted in Figure 1. The lateral dimensions of the elastic film are $2L_x$ and $2L_y$, where $L_x = L_y = L$, without losing any generality. The elastic film is rigidly bonded to the substrate so that the displacements at the film−substrate interface are zero. The free surface of the film is in contact proximity with the contactor and undergoes deformations whenever the strength of the interactions exceed a threshold value. The vector $\boldsymbol{n}$ is the outward surface normal to the film surface. The patterned substrate landscape is defined by its amplitude β_p (= βh) and wavelength λ_p, the contactor pattern is defined by the amplitude ω_q (= ωd) and wavelength λ_q, and these are among the controlling parameters in this problem. The simulations are carried over a single contactor and substrate pattern wavelength as shown in the figure. However, the system is considered to be periodic and can be repeated over larger lengths. A parameter value of $\omega_q = 0$ represents the case of a flat contactor, whereas $\beta_p = 0$ represents the case of a flat substrate. It will be shown later that to carry out the study in computational plane it is necessary to consider a long-wave limit for substrate patterning, which basically considers that $\beta h/2L \ll 1$ or $\beta h/2L = \varepsilon$, where ε is a very small quantity that tends to 0.

An external voltage V is applied between the contactor and the substrate to generate electrostatic interactions. When the applied voltage V exceeds the critical voltage, V_c, the electrostatic forces between the film and the contactor become strong enough to deform the flat film and compete with the elastic restoring forces of the film. This results in buckling of the film surface.

The governing equation for electric potential that develops in the air gap and the film is given by $\nabla^2\psi^a = 0$ and $\nabla^2\psi^f = 0$, respectively.[30] When the gap distance in the assembly is considered to be much less than the lateral lengths of the film (or $(h + d)/2L \ll 1$) as is considered in the present case, the gradients of the potential and higher order derivatives in the lateral directions can be ignored when compared to the gradient in the transverse direction. Such a criteria is justified in the present case since $(h + d)/2L = \varepsilon(1 + (1/R))/\beta$ will tend to very small values as R (= h/d) takes very high values. The minimum value of R that can be considered is of the order of 1, and values of R below this will require very high voltages and will not be physically possible to sustain. Also, the values of β considered in the present study are finite and ≠0, and thus, the governing equation in this limit is given by

$$\psi^i_{zz} = 0 \tag{1}$$

for i = a,f, which satisfies the following boundary conditions:[30,47]

$$\begin{aligned} &\psi^a = 0 \text{ at } z = d + \omega_q \cos(k_q x) \\ &\psi^f = V \text{ at } z = -(h - \beta_p \cos(k_p x)) \\ &\psi^a = \psi^f \text{ at } z = \mathbf{u}\cdot\mathbf{n} \text{ (the film−air interface)} \\ &\epsilon_a \frac{d\psi^a}{dz} = \epsilon_f \frac{d\psi^f}{dz}, \text{ at } z = \mathbf{u}\cdot\mathbf{n} \end{aligned} \tag{2}$$

where $\mathbf{u}$ is the displacement vector, V is the applied voltage, ϵ_f is the dielectric constant of the film (= 2.3−2.8 for PDMS films), and ϵ_a is the dielectric constant of air which is often considered as 1. k_p, k_q are the wavenumbers of the substrate pattern and the contactor pattern, respectively, and are given by $k_p = 2\pi n_p/2L = 2\pi/\lambda_p$, $k_q = 2\pi n_q/2L = 2\pi/\lambda_q$, where n_p, n_q are the number of wavemodes of the substrate pattern and the contactor pattern, respectively.

Solution of the above Laplace equation eq 1 along with the boundary conditions eq 2 helps one to find the electric field in the air and the film as well as in finding the Maxwell stresses and the resulting conjoining pressure due to the electrostatic interaction $\phi = \partial\Delta G/\partial u$ that develop in the polymer film:[47]

$$\phi = \epsilon_0\left[\epsilon_f\left(\frac{d\psi^f}{dz}\right)^2 - \left(\frac{d\psi^a}{dz}\right)^2\right] \tag{3}$$

where ϵ_0 is the free-space permittivity (= 8.85×10^{-12} C^2/J·m).

From eq 3, one can find the value of ΔG in the film. The free energy due to interaction potential can also be obtained from the amount of energy that is stored in the capacitor system (as shown in Figure 1) and is given by

$$\Delta G = -\frac{1}{2}CV^2 \tag{4}$$

where C is the total capacitance provided by the air and the film system and is given by[58]

dx.doi.org/10.1021/la502933c | Langmuir 2014, 30, 12278−12286

$$\frac{1}{C} = \frac{1}{C^{f}} + \frac{1}{C^{a}} = \frac{(h - \beta_p \cos(k_p x) + \mathbf{u}\cdot\mathbf{n})}{\epsilon_0 \epsilon_f} + \frac{d + \omega_q \cos(k_q x)}{\epsilon_0} \quad (5)$$

Both the above approaches help to find the attractive electrostatic interaction potential as a function of the actual gap distance $d' = d + \omega_q \cos(k_q x)$ and local film thickness $h - \beta_p \cos(k_p x)$ and is represented by

$$\Pi_U(d' - \mathbf{u}\cdot\mathbf{n}) = -\frac{\epsilon_0 \epsilon_f V^2}{2[(\epsilon_f - 1)(d' - \mathbf{u}\cdot\mathbf{n}) + d' + (h - \beta_p \cos(k_p x))]} + \frac{B_h}{(d' - \mathbf{u}\cdot\mathbf{n})^8} \quad (6)$$

where, B_h is the Born repulsion constant.

For van der Waals interactions, the interaction potential takes the form:

$$\Pi_U(d' - \mathbf{u}\cdot\mathbf{n}) = -\frac{A_h}{12\pi(d' - \mathbf{u}.\ \mathbf{n})^2} + \frac{B_h}{(d' - \mathbf{u}\cdot\mathbf{n})^8} \quad (7)$$

Here, A_h is the Hamaker constant whose value lies in the range of 10^{-19}−10^{-21} J. The value of the Born repulsion constant B_h is set from the following two conditions: (a) At the equilibrium separation distance d_e, the excess force per unit area is zero, that is, $\Pi_U'(d_e) = 0$, and is repulsive at distances less than d_e. (b) At the equilibrium separation distance, the adhesive potential is equal to the adhesive energy of contact, that is, $\Pi_U(d_e) = \Delta G_0 (= -(A_h/12\pi h_e^2)$, where h_e = 0.158 nm for van der Waals interactions).

The stored elastic energy will try to resist any deformation caused by the interaction potential in an attempt to restore the film to its original configuration and this total elastic energy of the film is given by the expression:

$$\Pi_E = \int_v \frac{1}{2}\sigma_{ij}\epsilon_{ij}\, dV \quad (8)$$

where

$$\sigma = \frac{\partial \Pi_E}{\partial \epsilon} = 2\mu\left[\epsilon + \frac{\nu}{(1 - 2\nu)}(tr(\epsilon))I\right] \quad (9)$$

The parameter $\boldsymbol{\sigma}$ represents the stress tensor in the film, $\mathbf{I}$ is the identity tensor, $\boldsymbol{\epsilon}$ is the strain tensor and is defined as the symmetric part of $\nabla\mathbf{u}$, ν is the Poisson ratio and a value close to 0.5 is taken in this work to represent the almost incompressible films under consideration, and in this limit eq 8 can be recast in the following form:

$$\Pi_E = \int_S \frac{1}{2}\sigma_{ij}u_i n_j\, dS \quad (10)$$

The displacements that the free surface of the film undergoes in the direction of the outward normal $\boldsymbol{n}$ can be represented by its Fourier Series as

$$u_z(x, y, 0) = \sum_{n_x=0}^{2N_x-1}\sum_{n_y=0}^{2N_y-1} \alpha_{cc}(n_x, n_y)\cos(k_{n_x}x)\cos(k_{n_y}y) + \alpha_{cs}(n_x, n_y)\cos(k_{n_x}x)\sin(k_{n_y}y) + \alpha_{sc}(n_x, n_y)\sin(k_{n_x}x)\cos(k_{n_y}y) + \alpha_{ss}(n_x, n_y)\sin(k_{n_x}x)\sin(k_{n_y}y), \quad (11)$$

where α_{cc}, α_{cs}, α_{sc}, and α_{ss} are the amplitudes of the displacements of the film surface, and $k_{nx} = 2\pi n_x/2L$ and $k_{ny} = 2\pi n_y/2L$ denote the wavenumber of deformation in x and y direction, respectively.

The total energy ($\Pi_U + \Pi_E$) minimizing equilibrium displacement fields in the film is supposed to satisfy the Navier's equation in the bulk as given by

$$(1 - 2\nu)u_{l,mm} + u_{m,ml} = 0 \quad (12)$$

It is also required to satisfy the no-slip and the rigid boundary conditions at the film−substrate interface as given respectively by

$$u_m(x, y, -h + \beta_p \cos(k_p x)) = 0, \text{ where } m = x, y, z \quad (13)$$

as well as the shear free boundary conditions at the film−air interface as given by

$$\sigma_{zx}(x, y, 0) = 0 \quad \text{and} \quad \sigma_{zy}(x, y, 0) = 0 \quad (14)$$

The substrate considered here is a curved surface with sinusoidal profile. Hence, we introduce a boundary-fitted coordinate transformation to transform the nonlinear wavy geometry in the physical plane (x,y,z) into a rectangular grid in the computational plane (ξ,η,γ) which renders the equations amenable for numerical analysis by separation of variables.

Coordinate Transformation. The choice of the new coordinate lines is such that the wavy substrate pattern now becomes a coordinate line γ = constant. The coordinates in the physical space are transformed to the computational space using the following equations:

$$\xi = \xi(x, y, z) = x,\ \eta = \eta(x, y, z) = y$$
$$\gamma = \gamma(x, y, z) = \frac{z}{f_p},\ \text{where } f_p = -h + \beta_p \cos(k_p x) \quad (15)$$

Thus, the film-substrate boundary $z = -h+\beta_p \cos(k_p x)$ gets transformed to $\gamma = 1$ and the film−air interface is given by $\gamma = 0$.

The displacement field in the transformed coordinates is considered to have the following variable separable form in terms of the single Fourier modes in both ξ and η direction as given below:

$$\begin{aligned} u_x(x, y, z) &= U_\xi(\xi, \eta, \gamma) \\ &= \tilde{U}_\xi(\gamma)[\sin(k_\xi\xi)\cos(k_\eta\eta) + \sin(k_\xi\xi)\sin(k_\eta\eta) \\ &\quad - \cos(k_\xi\xi)\cos(k_\eta\eta) - \cos(k_\xi\xi)\sin(k_\eta\eta)] \\ u_y(x, y, z) &= U_\eta(\xi, \eta, \gamma) \\ &= \tilde{U}_\eta(\gamma)[\cos(k_\xi\xi)\sin(k_\eta\eta) - \cos(k_\xi\xi)\cos(k_\eta\eta) \\ &\quad + \sin(k_\xi\xi)\sin(k_\eta\eta) - \sin(k_\xi\xi)\cos(k_\eta\eta)] \\ u_z(x, y, z) &= U_\gamma(\xi, \eta, \gamma) \\ &= \tilde{U}_\gamma(\gamma)[\cos(k_\xi\xi)\cos(k_\eta\eta) + \cos(k_\xi\xi)\sin(k_\eta\eta) \\ &\quad + \sin(k_\xi\xi)\cos(k_\eta\eta) + \sin(k_\xi\xi)\sin(k_\eta\eta)] \end{aligned} \quad (16)$$

The above-mentioned equilibrium displacement fields are supposed to satisfy stress equilibrium equations of eq 12 transformed to computational plane using the transformation of the derivatives of eqs A1−A3 as given in the Supporting Information. It is reported in the prior works on elastic films cast on patterned substrates that the instability length scales are mainly influenced by the substrate pattern amplitude β_p and are virtually independent of the substrate pattern wavelength λ_p (except in some pockets of λ_p).[43,44]

Hence, we assume a long-wave limit of the substrate patterning (i.e., $k_p \to 0$) for simplifying the stress-equilibrium equations of eqs A4−A6 in the computational plane. The stress equilibrium equations, thus, simplified are given in the Supporting Information. The transformed stress equilibrium conditions of eqs A7−A9 along with the perturbation fields of eq 16 lead to the following fourth-order differential equation in the transformed normal displacement field $\tilde{U}_\gamma(\gamma)$:

dx.doi.org/10.1021/la502933c | Langmuir 2014, 30, 12278−12286

$$\tilde{U}_\gamma^{iv}(\gamma) - 2k_n^2(-h+\beta_p)^2\,\tilde{U}_\gamma''(\gamma) + k_n^4(-h+\beta_p)^4\,\tilde{U}_\gamma(\gamma) = 0 \tag{17}$$

The form of eq 17 obtained from 3D displacement fields is exactly similar to that of 2D biharmonic equations obtained for flat elastic film,[43] with the exception that the wavenumber $k_n = k_x$ in the 2D is now replaced by an equivalent wavenumber $k_n = (k_{n_\xi}^2 + k_{n_\eta}^2)^{1/2}$ and the thickness of the film is replaced by the effective thickness $h(1-\beta)$ for patterned substrate and the negative sign appears because of the coordinate transformation where the dimensionless domain in the direction of the interactions range from 0−1 rather than 0 to −1. The solution of the above fourth order differential equation, $\tilde{U}_\gamma(\gamma)$ and all the other components of displacement can be obtained by solving for the displacement and stress boundary conditions in the transformed coordinates and is given in the Supporting Information.

The normal traction at the surface can be evaluated from the normal stresses at the top surface of the film and in the tranformed coordinates it is given by

$$\sigma_{zz}(\xi, \eta, 0) = 2\mu k_n S'(k_n)\, U_\gamma(\xi, \eta, 0) \tag{18}$$

where

$$S'(k_n) = \frac{1 + (3-4\nu)\cosh(2k_n f_r) + 2(k_n f_r)^2 + 4(1-2\nu)(1-\nu)}{-2(1-\nu)((3-4\nu)\sinh(2k_n f_r) + 2k_n f_r)} \tag{19}$$

where $f_r = -h + \beta_p$.

A balance of forces gives the traction at the surface as[43,41,44]

$$\sigma_{zz}(x, y, 0) = -\partial\Pi_u/\partial u_z \tag{20}$$

The critical conditions, namely, the minimum separation distance, the smallest voltages, and the wavemodes of deformation that the film will experience at the onset of instability, can be obtained by finding the minimum of LHS of eq 20 which leads to the following condition for electrostatic interactions:

$$\frac{h\epsilon_0\epsilon_f(\epsilon_f-1)^2V_c^2}{\mu(h(1-\beta\cos(k_p\xi)) + \epsilon_f d')^3} = \frac{6.22}{(1-\beta)} \tag{21}$$

and for van der Waals interactions it is

$$\frac{A_h h}{2\pi\mu d_c^4} = \frac{6.22}{(1-\beta)} \tag{22}$$

The total energy consisting of the interaction energy (from either electrostatic interactions of eq 6 or van der Waals interactions of eq 7) and the elastic energy of eq 10, where only the contributions from the top surface are accountable (the other surfaces being periodic or having zero displacements do not have any contribution), when expressed in terms of all the Fourier coefficients of displacements have the following form in transformed coordinates:

$$\begin{aligned}\Pi &= \Pi_U + \Pi_E \\ &= \int_0^{2L}\int_0^{2L} \Pi_U\Bigg(d - \sum_{n_\xi=0}^{2N_\xi-1}\sum_{n_\eta=0}^{2N_\eta-1}(\alpha_{cc}(n_\xi, n_\eta)\cos(k_{n_\xi}\xi) \\ &\quad \times \cos(k_{n_\eta}\eta) + \alpha_{cs}(n_\xi, n_\eta)\cos(k_{n_\xi}\xi)\sin(k_{n_\eta}\eta) \\ &\quad + \alpha_{sc}(n_\xi, n_\eta)\sin(k_{n_\xi}\xi)\cos(k_{n_\eta}\eta) + \alpha_{ss}(n_\xi, n_\eta) \\ &\quad \times \sin(k_{n_\xi}\xi)\sin(k_{n_\eta}\eta)\Bigg)\mathrm{d}\xi\,\mathrm{d}\eta + \frac{\mu}{h}L^2 \\ &\quad \times \Bigg[\sum_{n_\xi=0}^{2N_\xi-1}\sum_{n_\eta=0}^{2N_\eta-1} S''(k_n)(\alpha_{cc}^2(n_\xi, n_\eta) + \alpha_{cs}^2(n_\xi, n_\eta) \\ &\quad + \alpha_{sc}^2(n_\xi, n_\eta) + \alpha_{ss}^2(n_\xi, n_\eta))\Bigg]\end{aligned} \tag{23}$$

where

$$S''(k_n) = S'(k_n)(1 + \delta(n_\xi, 0))(1 + \delta(n_\eta, 0)) \tag{24}$$

Here, δ is the Kronecker delta.

The actual morphology of the top surface can be obtained by finding the optimum Fourier coefficients that minimize the total energy of eq 23. This is done by employing a conjugate gradient method in the simulations.

RESULTS AND DISCUSSION

The parameters used for the simulations are $\mu = 0.1$ MPa, mean film thickness h is 1 μm, and mean substrate amplitude β is in the range of 0−0.6. In the earlier works on confined and freely standing elastic films, it was reported that the surface energy effects are felt only when the surface tension parameter $\Gamma/(\mu h) > 1$ (where Γ is the surface energy of the film).[26,56] In the present work, for the film properties considered, the value of $\Gamma/(\mu h)$ is always less than 1. Hence the surface energy effects have been neglected in the study. The x−y domain considered is of size $32h \times 32h$, and simulations were performed by considering 128×128 Fourier coefficients.

We first present in Figure 2 the pattern formation in soft thin elastic films cast on sinusoidally patterned substrates when they are subjected to van der Waals interactions from a flat contactor at a critical separation distance calculated from eq 22. The substrate patterns are considered to have amplitude ratios β = 0.1, 0.3, 0.5, and 0.6 in Figure 2A−D, respectively. In all the figure,s the darkest regions correspond to the areas of the film close to contact with the contactor and the lightest regions correspond to the areas that are farthest away. It can be observed from Figure 2 that labyrinthine patterns are formed at critical separation distance and exist throughout the lateral length of the film when purely van der Waals interactions are present. As β increases, the number of columns (marked by darker regions) making close contact with the contactor is found to increase.

In the inset of each figure, the magnitude of the Fourier coefficients is plotted against the Fourier modes $n_x \times n_y$. The presence of a dark quarter ringlike structure indicates the existence of a dominant wavelength of instability. The dominant wavelength is given by the ratio of the characteristic length $2L$ to the characteristic wavemode $(n_x^2 + n_y^2)^{1/2}$) picked from the coordinates of the ring structure. As β increases, the dominant length scale of instability decreases (as shown in the Figure 2), visible from the fact that the quarter ring in the inset shifts farther away from the origin. Thus, the dominant length

dx.doi.org/10.1021/la502933c | Langmuir 2014, 30, 12278−12286

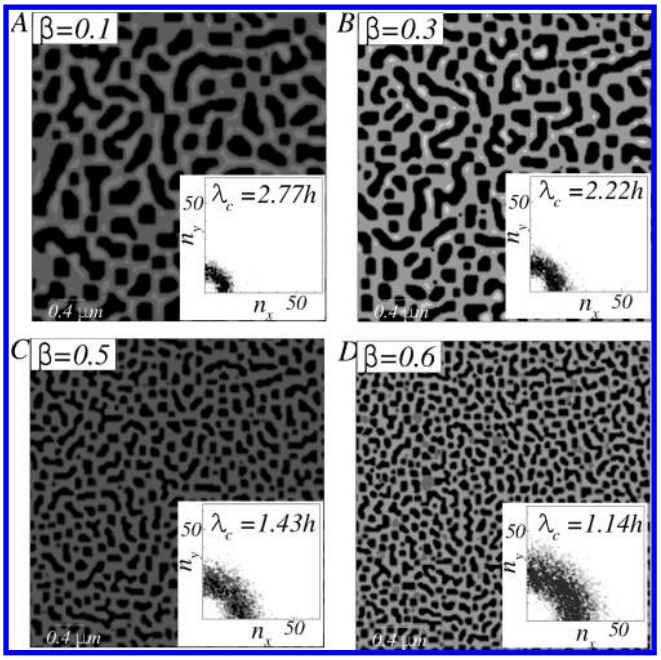

Figure 2. Morphologies of the labyrinthine patterns formed with van der Waals interactions in films cast on sinusoidally patterned substrates with different amplitudes β and in contact proximity of an external flat contactor. It can be seen that λ_c decreases as β increases. The darkest regions correspond to the areas of contact of the film with the contactor and the lightest regions correspond to the areas of the film that are farther away from the contactor. Figures in the inset show the variation of the Fourier amplitudes with respect to the Fourier modes n_x and n_y. Film contactor parameters used in the simulations: $\omega = 0$, $A_h = 10^{-20}$ J, $h = 0.1$ μm, $\mu = 0.1$ MPa.

scale of instability λ_c decreases as shown in the figure and is in close agreement with the predictions of linear stability analysis of $\lambda_c = 2.96(1 - \beta)h$.[44] Figure 2A represents the results for the case of a a nearly flat substrate. Though the instability length scales decrease as the substrate pattern amplitudes β increase, there is no long-range order present in the patterns formed. This is typical for the short-range van der Waals interactions which fail to introduce long-range order in the patterns. Also the patterns formed are highly disordered compared to those formed when flat substrates are used[56] as can be visualized from the diffuse state of the quarter ring formed in the insets of Figure 2 as β increases.

It was reported in the previous works that suppressing the van der Waals interactions and introducing electrostatic interactions induced long-range order into the patterns.[23] In what follows, we have focused on identifying the morphologies of the electric field induced patterns at the incipience of instability, the effect of the substrate amplitude, and the ratio of mean film thickness h and air gap d on the patterns that are formed and track the evolution of the morphologies as the applied voltage is ramped up. The electric field strength varies throughout the lateral direction due to variation of local separation distance of the substrate and the contactor ($(d' + h - \beta\cos(k_p x))$ values); hence, the critical voltage required varies throughout the lateral length of the film. The minimum critical voltage corresponding to $h = h(1 - \beta)$ will be sufficient only to deform very small region in the film; that is, only the negligile portions of the film that lie above the crest of the substrate while the maximum critical voltage corresponding to $h = h(1 + \beta)$ causes zones of least local film thickness to jump into total contact. Also, these minimum and maximum critical voltages differ as β varies. Hence, for flat contactor systems, we chose the critical voltage to be that corresponding to the mean film thickness h such that for a given h/d ratio films with different substrate roughnesses experience the same induced voltage so that we can analyze the patterns formed at a constant applied voltage for varying substrate roughnesses. We refer to this critical voltage at mean film thickness as $V_{c,h}$ in the present work (which can be obtained by inserting $\beta = 0$ in eq 21).

Figure 3 shows the morphologies of the patterns formed due to electrostatic interactions between sinusoidally patterned

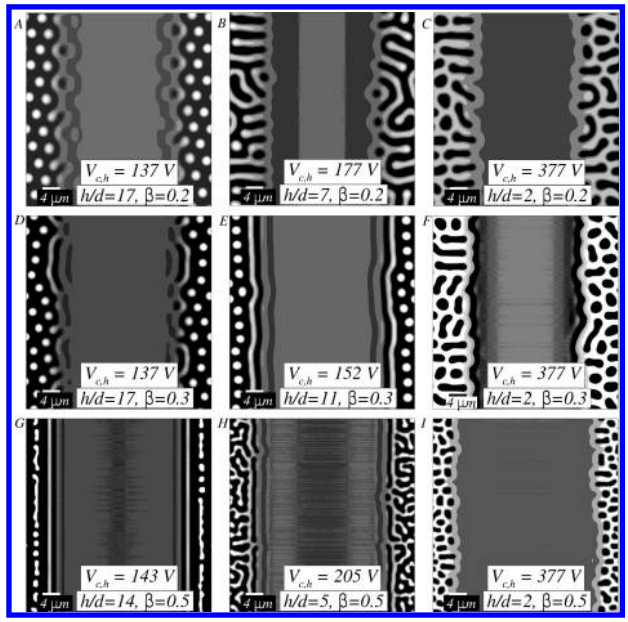

Figure 3. Morphologies of the patterns formed at the critical voltage with respect to the mean film thickness $V_{c,h}$ with electrostatic interactions for different ratios of β and h/d. When the values of h/d are large (A,D,G), the morphologies predominantly consist of cavities; for intermediate values of h/d, there is a transition to labyrinthine patterns (B,E,H). At very small values of h/d, the morphology consists of columns (C,F,I). Film, contactor parameters used in the simulations: $\omega = 0$, $\epsilon_f = 2.5$, $h = 1$ μm, $\mu = 0.1$ MPa.

substrate with different substrate amplitude ratios (β) and a flat contactor ($\omega = 0$) situated at a fixed gap distance d from the free surface of the film. The simulations were initiated with the critical voltage corresponding to the mean film thickness h, $\epsilon_f = 2.5$. In these, it can be observed that the pattern formation is confined to the zones where the local film thickness is less, or conversely, where locally stronger interactions are felt due to local variation in film thicknesses unlike the uniformly distributed patterns formed from van der Waals interactions (refer to Figure 2).

It is observed that when the values of air gap distances are small i.e. at large values of h/d, the morphology consists of cavities. For example, in Figure 3A for $\beta = 0.2$, we see that when $h/d = 17$, cavities are formed. For smaller values of β, the cavities are ordered in hexagonal pattern as was observed for flat substrates.[23] And as β increases the order is lost, though more number of columns can now be packed in the same domain length (e.g., there are 13 cavities in Figure 3D for $\beta = 0.3$ compared to 12 cavities in Figure 3A for $\beta = 0.2$). When β is increased further, the number of cavities gives the appearance of a striped structure as shown in Figure 3G. On the other

dx.doi.org/10.1021/la502933c | Langmuir 2014, 30, 12278−12286

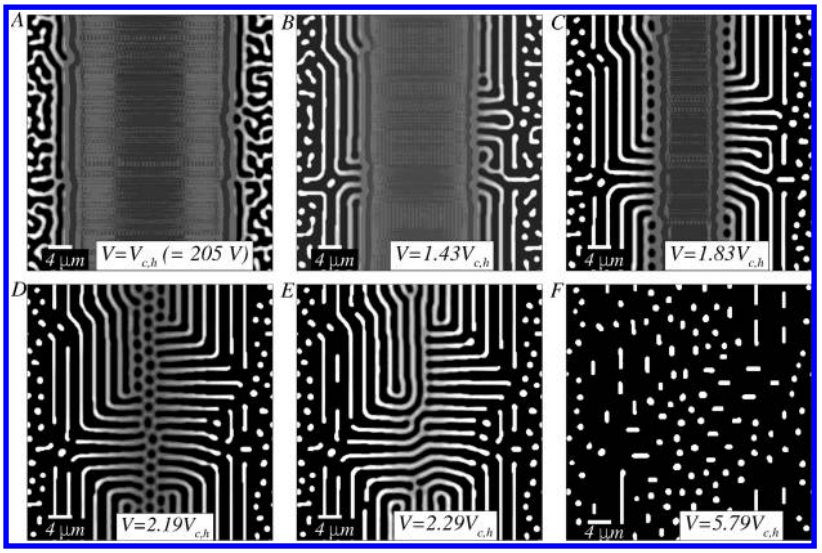

Figure 4. Morphologies of the patterns formed during various stages of evolution starting from the critical voltage $V_{c,h}$ with $\beta = 0.5$, $h/d = 5$. Striped patterns of (A) are found to evolve to three phase coexisting structures of cavities, stripes, and columns (B–D). On further evolution, circuit board patterns are formed in (E) which later give chaotically spaced cavities (F). Film, contactor parameters used in the simulations: same as in Figure 3.

hand, when h/d is very less, one obtains columnar structures as shown in Figure 3C, F, and I, which increase in number as β increases. However, the columnar structures are not orderly packed even for smaller β which is in stark contrast with the well ordered patterns that are formed with the flat substrates.[23] In between these two regimes of columnar and cavity structures, there exists a striped morphology for intermediate values of h/d which are never found in isolation and always coexist with either the cavity phase or the columnar phase depending on the initial h/d ratio (see Figure 3B, E, and H). This two phase coexistence is because of lateral variation in the electric field caused by variation in local film thickness due to substrate patterning.

It can be seen that, like in flat substrates, there exist three morphological phases in the patterns formed with patterned substrates, namely, columns, stripes, and cavities. These patterns can be formed with much miniaturized length scales; however, they are now localized and the salient ordering of electric field induced patterns is completely lost.[23,45,46]

The patterns that were formed at $V_{c,h}$ in Figure 3 were evolved by ramping the voltage to see if the area that remained unpatterned because of higher local thicknesses (and consequently lower interaction strengths) in Figure 3 can experience interactions strong enough to deform it. The results of these simulations are shown in Figure 4. As the voltage is increased the striped patterns that are formed at critical voltages give rise to cavities at the outer edges where the local thickness of the film is less (Figure 4B). As the voltage is increased further, the patterned zones emerge radially inward as the local interaction strengths increase and the newer zones emerge in the previously unpatterned midsection by forming columnar patterns. This can be seen from Figure 4B–D that as the voltage is increased from $V = 1.43V_{c,h}$ to $V = 2.19V_{c,h}$, it is possible to pattern the entire film and also there is a three phase coexistence of the patterns, columns, stripes, and cavities. Such three phase coexistence has never been seen earlier in soft elastic films either with flat substrates or with patterned contactors where only distinct first order transitions were observed.[23] Such distinct morphologically structures are potentially useful in enhancing optical properties such as structural colors or antireflective properties of a surface.[13]

As the voltage is ramped up further to $V = 2.29V_{c,h}$, the columnar structures formed at the midsection merge either with the neighboring striped patterns or with neighboring columns to give rise to a continuous circuit-board-like patterns (see Figure 4E). The film breaks down into completely chaotic arrangement of cavities when the voltage is very high (see Figure 4F).

From Figure 4, it is evident that the patterned zone strongly influences the evolving zones, and it can be anticipated that the voltage at which the instabilities are first triggered should also have a great say in the morphological phases formed during evolution. For this, we started with a voltage $V = 1.4V_{c,h}$ which is much stronger than the critical voltage $V_{c,h}$ for the same parametric values of Figure 4. Figure 5A shows that the initial patterns are longitudinally striped and when they are allowed to evolve (by increasing applied voltage) the phenomenon of pattern evolution remains unchanged. The columnar structures are still formed in the emerging pattern zones; however, the columns, being in close proximity to each other, merge longitudinally to give rise to longitudinal stripes as can be seen from Figure 5B–D. Such uniform longitudinal stripes can be used in microfluidic devices,[11] solar cells,[9] and so forth. It is interesting to observe here that though the voltages in Figure 4D and E are the same as those of Figure 5C and D, in the former case the evolved patterns helped the formation of newer stripes in lateral direction, whereas in the current case the stripes cannot laterally interact with the columnar structures to merge and form circuit-board pattern. Thus, though both figures have similar interaction strengths in a film with similar properties, they give rise to strikingly different patterns.

It happens occasionally that one is required to isolate a single phase, usually columnar phase, for applications like gecko-pad inspired superadhesives.[59] It was reported in some of the works in the literature that when a patterned contactor is used instead of a flat contactor, the spatially nonuniform electric field aligns the patterns where the local air gap distances are the least for elastic films cast on flat substrates.[23,40] It can be presumed that if a contactor can be patterned in such a way that the lateral

dx.doi.org/10.1021/la502933c | Langmuir 2014, 30, 12278–12286

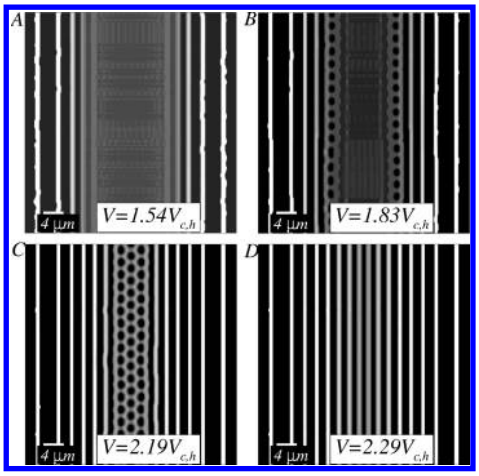

Figure 5. Morphologies of the patterns formed during various stages of evolution starting from a voltage greater that the critical voltage (with respect to the mean film thickness) $V = 1.4V_{c,h}$ with $\beta = 0.5$, $h/d = 5$. Initial longitudinal striped patterns of (A) give rise to intermediate patterns consisting columns sandwiched between the striped structures of (B) and (C). These on further evolution give longitudinal, well-ordered striped patterns (D). Film, contactor parameters used in the simulations: same as in Figure 4.

variation in film thickness due to substrate patterning is compensated by the lateral variation in air-gap due to contactor patterning, it might lead to regular, ordered patterning of the entire film whose length scales are still governed by the substrate pattern amplitude parameter β. For this to happen, the sinusoidal effects that arise due to substrate patterning and the contactor patterning should cancel each other out and this can happen only if $\lambda_p = \lambda_q$ and both the patterns are completely in phase. Such a condition can occur if $\epsilon_f d\omega = h\beta$ in eq 6. When this condition is satisfied, the true critical voltage (V_c) as calculated from eq 21 is used to carry out the simulations as the lateral variation in the electric field due to variation in substrate roughness is compensated by the roughness of the contactor. If this condition is applied, it can be seen that the localization of patterns can be totally prevented and the uniformly spaced columnar patterns that are formed are highly ordered and almost hexagonally packed as those found in flat contactor/flat substrate assemblies.[23] It can also be seen that the dominant wavelength decrease from $\lambda_c = 2.96h$ for $\beta = 0$ is reduced by almost 50% to $\lambda_c = 1.45h$ for $\beta = 0.5$ (Figure 6F). The pattern ordering can be further increased by increasing the value of h/d, that is, by reducing the air gap distance d between the film and the contactor for the same mean film thicknesses as can be seen by comparing the figures in both columns of Figure 6. Such compact lattice of columnar structures of the soft elastic films have potential use in applications where a large surface area of microstructures is required and conventional lithographic techniques fail to achieve this in a single batch and are very expensive to produce in smaller batches. The only issue with this assembly is that the requirement of the nondimensional parameter $\omega < 1$ places a restriction on the values of h/d that should be maintained to satisfy the above condition for nullifying sinusoidal effects. This can only happen if h/d ratios are very less, and thus, it appears that only miniaturized, uniformly distributed columnar structures can be formed at the critical voltages and other morphological phase may not be attainable.

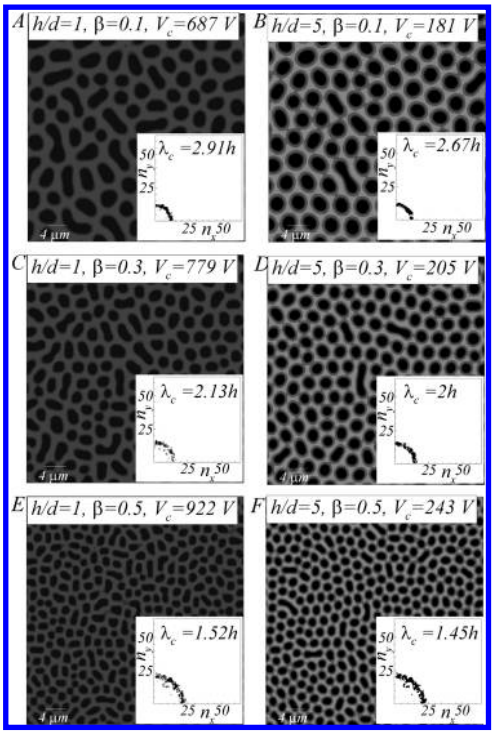

Figure 6. Morphologies of the patterns formed at the critical voltage V_c with electrostatic interactions and a patterned contactor which nullifies the sinusoidal effects. Highly ordered, almost hexagonally packed columnar structures are formed whose wavelength decreases from $2.67h$ for (B) to $1.45h$ for (F) as β increases. For a constant β, as h/d increases, the patterns become more ordered. Film, contactor parameters used in the simulations: $\epsilon_f = 2.8$, $h = 1$ μm, $\mu = 0.1$ MPa, $\omega = (\beta/\epsilon_f)(h/d)$.

However, this challenge can be overcome by allowing these columnar patterns that are formed at critical voltages in this in-phase assembly to evolve under higher applied electric fields. It is observed that there is a distinct first order transition from the columnar phase in Figure 7A to well-ordered stripes in Figure

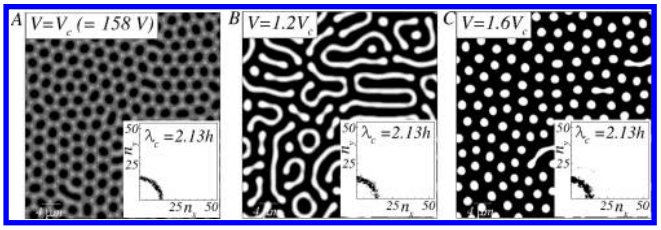

Figure 7. Morphologies of the patterns formed when the patterns formed at the critical voltage V_c are evolved by increasing the applied voltage for $\beta = 0.3$, $h/d = 9$ with patterned contactor. There is a transition from (A) ordered columnar patterns to (B) ordered striped patterns to (C) ordered cavities with the same dominant wavelength as the voltage increases. Film, contactor parameters used in the simulations: same as in Figure 6.

7B to ordered cavities in Figure 7C, both formed at reduced length scales of $2.13h$ for $\beta = 0.3$ compared to the flat substrate/flat contactor limit of $2.96h$. Needless to say, even more miniaturized, well-ordered, uniformly distributed, isolated morphological phases can be obtained at higher values of substrate amplitude parameter β.

dx.doi.org/10.1021/la502933c | Langmuir 2014, 30, 12278−12286

CONCLUSIONS

Miniaturization of patterns by a combination of substrate and contactor patterning is explored by virtue of 3D simulations of elastic films cast on unidirectional sinusoidally patterned substrates. A coordinate transformation method is used to transform the physical space to computational space yielding equations that are amenable to perform the simulations. The important findings are summarized below:

1. When an elastic film cast on a patterned substrate is in contact proximity with a rigid, flat contactor, smaller critical length scales of instability are achieved compared to those obtained with flat substrate $\lambda_c < 2.96h$. The length scales decrease with an increase in the substrate pattern amplitude. In the case of van der Waals interactions, the patterns are labyrinthine, noisy, lack long-range order, and thus have limited utility.
2. When electrostatic interactions are present between the flat contactor and the patterned substrate, the morphologies formed at critical voltages are strongly dependent on the initial air gap distances. At very small values of the air gap distances or large values of h/d, cavities are formed at critical voltages. The cavities are hexagonally ordered and have length scales $< 2.96h$. At much higher initial air gap distances of the order of the mean film thickness, columns are formed with characteristic spacing similar to that in the cavities morphology. However, the columns are no longer regularly packed as the cavities. In the intermediate ratios of h/d, stripes are formed; however, the patterns that are formed are always not isolated and are concentrated in the zones where the local interaction strengths are the highest.
3. As the patterns formed at the critical voltage are evolved by increasing the applied voltage, three phase morphological coexistence of very short-waved patterns throughout the area of the film is observed. The voltage at which the film is made to undergo deformation initially has a say in the stages of evolution, and strikingly different patterns can be obtained at the same evolved voltages.
4. When integrated with a prepatterned contactor and the sinusoidal effects introduced by the substrate patterning are made to commensurate by the contactor patterning, it becomes possible to have a uniform interaction field throughout the lateral directions and yet retain the signature miniaturization introduced by the substrate patterning. This indeed produces uniformly distributed, miniaturized columnar patterns at critical voltages which on evolution can give rise to uniform striped patterns and cavities as well.

These results help in unraveling for the first time coexistence of multiple phases of instabilities in a single, confined soft elastic film. They also suggest that great control can be achieved over not just the length scales but over the extent of patterning i.e. one can form localized patterns or uniformly distributed patterns, patterns with single morphological phase or multiple morphological phases in a single elastic film with the help of an externally tunable electric field. Very short waved (having wavelengths almost an order of magnitude less than those obtained with flat substrate - flat contactor assemblies reported so far), well-ordered patterns can be formed with the desired spatial variation which have huge potential for applications like microfluidic devices etc. Moreover the voltages reported are less than the breakdown voltage of air[60] and thus, it will be feasible to achieve the patterns experimentally.

ASSOCIATED CONTENT

Supporting Information

Transformation of equations from physical to computational plane and solution of fourth order differential equation in normal displacement. This material is available free of charge via the Internet at http://pubs.acs.org.

AUTHOR INFORMATION

Corresponding Author

*E-mail: jayati@chemical.iitd.ernet.in.

Notes

The authors declare no competing financial interest.

ACKNOWLEDGMENTS

The authors gratefully acknowledge the involvement of Chandrakant Khudsange in the initial stages of model development. The project was supported by the Department of Science & Technology, New Delhi.

REFERENCES

(1) Wang, C.-W.; Sinton, D.; Moffitt, M. G. Morphological control via chemical and shear forces in block copolymer self-assembly in the lab-on-chip. *ACS Nano* **2013**, *7*, 1424−1436.
(2) Curtis, A.; Wilkinson, C. Nantotechniques and approaches in biotechnology. *Trends Biotechnol.* **2001**, *19*, 97−101.
(3) Moroni, L.; de Wijn, J. R.; van Blitterswijk, C. A. Integrating novel technologies to fabricate smart scaffolds. *J. Biomater. Sci., Polym. Ed.* **2008**, *19*, 543−572.
(4) Yoo, D.; Wu, A.; Lee, J.; Rubner, M. F. New electro-active self-assembled multilayer thin films based on alternately adsorbed layers of polyelectrolytes and functional dye molecules. *Synth. Met.* **1997**, *85*, 1425.
(5) Yan, X.; Liu, G.; Dickey, M.; Willson, C. G. Preparation of porous polymer membranes using nano- or micro-pillar arrays as templates. *Polymer* **2004**, *45*, 8469−8474.
(6) Attia, R.; Pregibon, D. C.; Doyle, P. S.; Viovy, J.-L.; Bartolo, D. Soft microflow sensors. *Lab Chip* **2009**, *9*, 1213−1218.
(7) Salleo, A.; Wong, W. S.; Chabinyc, M. L.; Paul, K. E.; Street, R. A. Polymer Thin-Film Transistor Arrays Patterned by Stamping. *Adv. Funct. Mater.* **2005**, *15*, 1105−1110.
(8) Chabinyc, M. L.; Wong, W. S.; Salleo, A.; Paul, K. E.; Street, R. A. Organic polymeric thin-film transistors fabricated by selective dewetting. *Appl. Phys. Lett.* **2002**, *81*, 4260−4262.
(9) Krebs, F. C.; Fyenbo, J.; Jorgensen, M. Product integration of compact roll-to-roll processed polymer solar cell modules: methods and manufacture using flexographic printing, slot-die coating and rotary screen printing. *J. Mater. Chem.* **2010**, *20*, 8994−9001.
(10) Moctar, A. O. E.; Aubry, N.; Batton, J. Electro-hydrodynamic micro-fluidic mixer. *Lab. Chip* **2003**, *3*, 273−280.
(11) Gao, L.; McCarthy, T. J. The lotus effect explained: Two reasons why two length scales of topography are important. *Langmuir* **2006**, *22*, 2966−2967.
(12) Ueda, E.; Levkin, P. A. Emerging applications of superhydrophilic-superhydrophobic micropatterns. *Adv. Mater.* **2013**, *25*, 1234−1247.
(13) Kettle, J.; Hoyle, R. T.; Perks, R. M.; Dimov, S. Overcoming material challenges for replication of moth eye lenses using step and flash imprint lithography for optoelectronic applications. *J. Vac. Sci. Technol., B* **2008**, *26*, 1794−1799.
(14) Rath, S.; Heilig, M.; Port, H.; Wrachtrup, J. Periodic organic nanodot patterns for optical memory. *Nano Lett.* **2007**, *7*, 3845−3848.

(15) Black, C. T.; Ruiz, R.; Breyta, G.; Cheng, J. Y.; Colburn, M. E.; Guarini, K. W.; Kim, H.-C.; Zhang, Y. Polymer self assembly in semiconductor microelectronics. *IBM J. Res. Dev.* **2007**, *51*, 605−633.
(16) Mönch, W.; Herminghaus, S. Elastic instability of rubber films between solid bodies. *Europhys. Lett.* **2001**, *53*, 525−531.
(17) Shenoy, V.; Sharma, A. Pattern Formation in a Thin Solid Film with Interactions. *Phys. Rev. Lett.* **2001**, *86*, 119.
(18) Shenoy, V.; Sharma, A. Stability of a thin elastic film interacting with a contactor. *J. Mech. Phys. Solids* **2002**, *50*, 1155−1173.
(19) Sarkar, J.; Shenoy, V.; Sharma, A. Patterns, forces, and metastable pathways in debonding of elastic films. *Phys. Rev. Lett.* **2004**, *93*, 018302.
(20) Sarkar, J.; Sharma, A.; Shenoy, V. Adhesion and debonding of soft elastic films: Crack patterns, metastable pathways, and forces. *Langmuir* **2005**, *21*, 1457−1469.
(21) Sarkar, J.; Sharma, A.; Shenoy, V. Adhesion and debonding of soft elastic films on rough and patterned surfaces. *J. Adhes.* **2005**, *81*, 271−295.
(22) Arun, N.; Sharma, A.; Shenoy, V. B.; Narayan, K. S. Electric-field-controlled surface instabilities in soft elastic films. *Adv. Mater.* **2006**, *18*, 660−663.
(23) Sarkar, J.; Sharma, A.; Shenoy, V. B. Electric-field induced instabilities and morphological phase transitions in soft elastic films. *Phys. Rev. E* **2008**, *77*, 031604.
(24) Sarkar, J.; Shenoy, V.; Sharma, A. Spontaneous surface roughening induced by surface interactions between two compressible elastic films. *Phys. Rev. E* **2003**, *67*, 031607.
(25) Arun, N.; Sharma, A.; Pattader, P. S. G.; Banerjee, I.; Dixit, H. M.; Narayan, K. S. Electric-Field-Induced Patterns in Soft Viscoelastic Films: From long waves of viscous liquids to short waves of elastic solids. *Phys. Rev. Lett.* **2009**, *102*, 254502.
(26) Sarkar, J.; Sharma, A. A Unified Theory of Instabilities in Viscoelastic Thin Films: From wetting to confined films, from viscous to elastic films, and from short to long waves. *Langmuir* **2010**, *26*, 8464−8473.
(27) Reiter, G. Dewetting of thin polymer films. *Phys. Rev. Lett.* **1992**, *68*, 75−80.
(28) Seeman, R.; Herminghaus, S.; Jacobs, K. Dewetting patterns and molecular forces: A reconciliation. *Phys. Rev. Lett.* **2001**, *86*, 5534.
(29) Kargupta, K.; Sharma, A. Creation of ordered patterns by dewetting of thin films on homogeneous and heterogeneous substrates. *J. Colloid Interface Sci.* **2002**, *245*, 99−115.
(30) Verma, R.; Sharma, A.; Kargupta, K.; Bhaumik, J. Electric field induced instability and pattern formation in thin liquid films. *Langmuir* **2005**, *21*, 3710−3721.
(31) Mukherjee, R.; Sharma, A.; Patil, G.; Faruqui, D.; Pattader, P. S. G. Soft lithography meets self-organization: Some new developments in meso-patterning. *Bull. Mater. Sci.* **2008**, *31*, 249−261.
(32) Yuan, D.; Lasagni, A.; Hendricks, J. L.; Martin, D. C.; Das, S. Patterning of periodic nano-cavities on PEDOT−PSS using nano-sphere-assisted near-field optical enhancement and laser interference lithography. *Nanotechnology* **2012**, *23*, 015304.
(33) Ghatak, A.; Mahadevan, L.; Chung, J. Y.; Chaudhury, M. K.; Shenoy, V. Peeling from a biomimetically patterned thin elastic film. *Proc. R. Soc. London, Ser. A* **2004**, *460*, 2725−2735.
(34) Ghatak, A.; Chaudhury, M. K.; Shenoy, V.; Sharma, A. Meniscus instability in a thin elastic film. *Phys. Rev. Lett.* **2000**, *85*, 4329.
(35) Ghatak, A.; Chaudhury, M. K. Adhesion-induced instability patterns in thin confined elastic film. *Langmuir* **2003**, *19*, 2621−2631.
(36) Chakrabarti, A.; Chaudhury, M. K. Direct measurement of the surface tension of a soft elastic hydrogel: Exploration of elastocapillary instability in adhesion. *Langmuir* **2013**, *29*, 6926−6935.
(37) Tomar, G.; Sharma, A.; Shenoy, V.; Biswas, G. Surface instability of confined elastic bilayers: Theory and simulations. *Phys. Rev. E* **2007**, *76*, 011607.
(38) Yoon, J.; Ru, C. Q.; Mioduchowski, A. Surface instability of a bilayer elastic film due to surface van der Waals forces. *J. Appl. Phys.* **2005**, *98*, 113503.
(39) Mukherjee, R.; Pangule, R.; Sharma, A.; Tomar, G. Contact instability of elastic bilayers: Miniaturization of instability patterns. *Adv. Funct. Mater.* **2007**, *17*, 2356−2364.
(40) Mukherjee, R.; Sharma, A. Creating self-organized submicrometer contact instability patterns in soft elastic bilayers with a topographically patterned stamp. *ACS Appl. Mater. Interfaces* **2012**, *4*, 355−362.
(41) Annepu, H.; Sarkar, J. Squeezing instabilities and delamination in elastic bilayers: A linear stability analysis. *Phys. Rev. E* **2012**, *86*, 051604.
(42) Mukherjee, R.; Pangule, R. C.; Sharma, A.; Banerjee, I. Contact instability of thin elastic films on patterned substrates. *J. Chem. Phys.* **2007**, *127*, 064703.
(43) Sarkar, J.; Annepu, H.; Sharma, A. Contact instability of a soft elastic film bonded to a patterned substrate. *J. Adhes.* **2011**, *87*, 214−234.
(44) Annepu, H.; Sarkar, J.; Basu, S. Pattern formation in soft elastic films cast on periodically corrugated surfaces—A linear stability and finite element analysis. *Modell. Simul. Mater. Sci. Eng.* **2014**, *22*, 055003.
(45) Schäffer, E.; Thurn-Albrecht, T.; Russell, T. P.; Steiner, U. Electrically induced structure formation and pattern transfer. *Nature (London, U.K.)* **2000**, *403*, 874−877.
(46) Schäffer, E.; Thurn-Albrecht, T.; Russell, T. P.; Steiner, U. Electrohydrodynamic instabilities in polymer films. *Europhys. Lett.* **2001**, *53*, 518−524.
(47) Shankar, V.; Sharma, A. Instability of the interface between thin fluid films subjected to electric fields. *J. Colloid Interface Sci.* **2004**, *274*, 294−308.
(48) Gambhire, P.; Thaokar, R. M. Linear stability analysis of electrohydrodynamic instabilities at fluid interfaces in the small feature limit. *Eur. Phys. J. E* **2011**, *34*, 84(1)−(12).
(49) Gambhire, P.; Thaokar, R. M. Role of conductivity in the electrohydrodynamic patterning of air-liquid interfaces. *Phys. Rev. E* **2012**, *86*, 036301.
(50) Wang, Q.; Zhang, L.; Zhao, X. Creasing to cratering instability in polymers under ultrahigh electric fields. *Phys. Rev. Lett.* **2011**, *106*, 118301.
(51) Wang, Q.; Zhao, X. Creasing-wrinkling transition in elastomer films under electric fields. *Phys. Rev. E* **2013**, *88*, 042403.
(52) Bandyopadhyay, D.; Sharma, A.; Shankar, V. Instabilities and pattern miniaturization in confined and free elastic-viscous bilayers. *J. Chem. Phys.* **2008**, *128*, 154909.
(53) Bandyopadhyay, D.; Sharma, A.; Thiele, U.; Reddy, P. D. S. Electric-field-induced interfacial instabilities and morphologies of thin viscous and elastic bilayers. *Langmuir* **2009**, *25*, 91089118.
(54) Bandyopadhyay, D.; Sharma, A.; Shankar, V. Electric-field and contact-force-induced tunable patterns in slipping soft elastic films. *Europhys. Lett.* **2010**, *89*, 36002.
(55) Bandyopadhyay, D.; Sharma, A.; Shankar, V. Electric field and van der Waals force induced instabilities in thin viscoelastic bilayers. *Phys. Fluids* **2012**, *24*, 074106.
(56) Gonuguntla, M.; Sharma, A.; Sarkar, J.; Subramanian, S. A.; Ghosh, M.; Shenoy, V. Contact Instability in Adhesion and Debonding of Thin Elastic Films. *Phys. Rev. Lett.* **2006**, *97*, 018303.
(57) Gonuguntla, M.; Sharma, A.; Subramanian, S. A. Elastic contact induced self-organized patterning of hydrogel films. *Macromolecules* **2006**, *39*, 3365−3368.
(58) Schäffer, E. Instabilities in thin polymer films: Structure formation and pattern transfer. Ph.D. Thesis, University of Konstanz, 2001.
(59) Northen, M. T.; Turner, K. L. A batch fabricated biomimetic dry adhesive. *Nanotechnology* **2005**, *16*, 1159.
(60) Klas, M.; Matejčík, S.; Radjenović, B.; Radjenović, M. R. Experimental and theoretical studies of the breakdown voltage characteristics at micrometre separations in air. *Europhys. Lett.* **2011**, *95*, 35002.